A Fast Protection of Multi-terminal HVDC System Based on Transient Signal Detection

Liu, Lian; Liu, Zhou; Popov, Marjan; Palensky, Peter; van der Meijden, Mart

DOI
10.1109/TPWRD.2020.2979811

Publication date
2020

Document Version
Final published version

Published in
IEEE Transactions on Power Delivery

Citation (APA)
Liu, L., Liu, Z., Popov, M., Palensky, P., & van der Meijden, M. (2020). A Fast Protection of Multi-terminal HVDC System Based on Transient Signal Detection. *IEEE Transactions on Power Delivery*, *36*(1), 43-51. Article 9031399. https://doi.org/10.1109/TPWRD.2020.2979811

A Fast Protection of Multi-Terminal HVDC System Based on Transient Signal Detection

Lian Liu, Zhou Liu, *Senior Member, IEEE*, Marjan Popov, *Senior Member, IEEE*, Peter Palensky, *Senior Member, IEEE*, and Mart A. M. M. van der Meijden, *Member, IEEE*

***Abstract*—HVDC technologies are widely acknowledged as one of solutions for the interconnection of renewable energy resources with the main electric power grid. The application of the latest modular multi-level converter (MMC) makes power conversion much more efficient. Due to the relatively low impedance in a DC system, DC fault currents may rise to an extremely high level in a short period of time, which can be very dangerous for HVDC converters. To improve the sustainability and security of electricity transmission, protection solutions for HVDC systems are being developed. Nevertheless, they have various drawbacks on fault signal detection and timely clearance. This paper proposes a protection method that provides a fast and reliable solution addressing those drawbacks. A protection algorithm based on travelling wave simulation and analysis is proposed to detect abrupt transient signals. The algorithm shows high efficiency, reliability, selectivity and has low sampling frequency requirements. The proposed protection method has been validated through a cyber-physical simulation platform, developed using a real-time digital simulator (RTDS) and IEC 61850 communication links. The obtained results show that the proposed method has good potential for practical applications.**

***Index Terms*—Electromagnetic transients (EMT), high voltage direct current (HVDC), modular multi-level converter (MMC), protection, real time digital simulator (RTDS), signal processing, voltage source converter (VSC), IEC 61850.**

I. Introduction

HIGH voltage direct current (HVDC) technology is a proven solution for the connection of the increasing number of renewable power resources, e.g., offshore and onshore wind farms, which help to improve the sustainability of the energy supply. To enhance the robustness and flexibility of HVDC networks, it is proposed to use multi-terminal HVDC (MTDC) systems to integrate available HVDC links. The MTDC system is based on voltage source converters (VSC). Examples of this type of HVDC systems include the North Sea Transnational Grid [1] in Europe and Zhoushan DC grid in China [2].

HVDC converters are susceptible to faults due to the low impedance of the DC network. Large fault currents can easily damage the anti-paralleled diodes in the converter bridge, which may result in a collapse of the entire electrical network. For this reason, VSC HVDC protection is an area of intense research activity.

To reduce the vulnerability of VSC HVDC systems to DC faults, a full-H bridge MMC converter and some of its variants [3], in combination with DC circuit breakers (DCCB), can be used to isolate DC faults in an MTDC system. However, because of the relatively high cost and power losses, their application is not currently widespread.

Proposed protection methods of HVDC networks are given in [4]–[11]. The proposed methods can be divided into two categories: Unit protection and non-unit protection. Unit protection requires communication between each relay unit for a defined protection zone. For the methods based on differential current [4] and wavelet transform [5], the signals at two terminals must be compared. The main disadvantage of this category is that the fault detection algorithm heavily depends on the communication channel between remote ends in the system. As the communication link in HVDC line is hard to be built due to its long distance and the time delay could not be neglected. It is difficult to use this type of protection as main protection. By contrast, non-unit protection does not require remote communication, since it does not have fixed protection zones, and the fault detection is fully achieved by collecting and processing local information. Typical examples of this protection concept can be found in [6]–[8]. In [6], the protection concept makes use of the Stationary Wavelet Transform (SWT). Since each level's output of SWT contains the same number of samples as the input, this method has high redundancy. The non-unit protection reported in [7] is verified on a point-to-point HVDC network, so its applicability to MTDC systems is not yet proven. Protection based on voltage derivative in [8] needs a high sampling frequency of 100 kHz. Whilst high sampling frequencies are not an issue today due to the advanced development of fast signal processing technology, it is still preferable to develop protection methods with lower sampling frequency requirements.

Non-unit protection also contains distance protection, as described in [9]. The main technique is to approximate the frequency-dependent features of a cable or an overhead line

Manuscript received October 22, 2018; revised July 5, 2019, October 14, 2019, and February 7, 2020; accepted February 21, 2020. Date of publication March 10, 2020; date of current version January 22, 2021. Paper no. TPWRD-01244-2018. *(Corresponding author: Zhou Liu).*

Lian Liu is with Prysmian Group, 2627 AN Delft, The Netherlands (e-mail: lian.liu@prysmiangroup.com).

Zhou Liu is with the Department of Energy Technology, Aalborg University, 9220 Aalborg East, Denmark (e-mail: zli@et.aau.dk).

Marjan Popov and Peter Palensky are with the Faculty of EEMCS, Delft University of Technology, 2628 CD Delft, The Netherlands (e-mail: m.popov@ieee.org; p.palensky@tudelft.nl).

Mart A. M. M. van der Meijden is with TSO TenneT and the Faculty of EEMCS, Delft University of Technology, 2628 CD Delft, The Netherlands (e-mail: m.a.m.m.vandermeijden@tudelft.nl).

Color versions of one or more of the figures in this article are available online at http://ieeexplore.ieee.org.

Digital Object Identifier 10.1109/TPWRD.2020.2979811

(OHL) in the time domain with finite impulse response (FIR) filters. However, curve fitting can cause considerable errors. The boundary protection method as reported in [10] is much more suitable for line commuted converters (LCC), as it makes use of the firing angles as an input. A fast protection and fault location method based on the rate of change of voltage (ROCOV) are proposed in [11]. However, it does not analyze the influence of the converter's arm reactor. In addition, the ROCOV will be affected by the sampling frequency and the noise of the signal. There is also research work in which the fault detection is based on a combination of measured current and voltage derivatives [12]. Although it can provide higher reliability, it requires high sampling frequency to record the traveling wave.

To achieve reliable protection with low sampling requirements, this paper proposes a fast and robust protection method without making use of remote communication. The developed method utilizes incident surges caused by faults. Firstly, the transient phenomena at the inductive terminals of neighboring cables are simulated and analyzed. Secondly, based on the transient phenomena, two criteria are proposed to characterize the faults in the protection zones. Then, according to the sensitivity analysis, the thresholds of these criteria are determined, which can guarantee selectivity of the proposed method. Finally, the simulation verifies that a low sampling frequency is sufficient for fast fault detection, and the proposed method can be implemented for primary protection.

The structure of the paper is as follows. Section II discusses the current and the voltage behavior caused by an incident surge, and the analysis is based on simulation. In Section III, the key algorithm of the protection is demonstrated. Section IV deals with the test system represented in the RTDS environment, whilst in Section V, the performance of the protection method is shown and discussed. The paper summarizes the conclusions in Section VI.

II. DC Current and Voltage Responses After DC Fault

A. MMC-Based MTDC System

In this section, the DC current and voltage of an MTDC network after a fault occurrence are simulated and discussed. To ensure accurate simulation results, an MTDC network is modeled in detail. The MTDC network comprises four half-bridge (HB) MMC converters. An inductor-capacitor-inductor (LCL) circuit is implemented on the AC-side of each converter bridge to limit the fault current. The LCL MMC converter is designed and operated as described in [13]. The configuration of the MTDC system is shown in Fig. 1, and the control modes of each converter are listed in Table I. Although the adopted MMC efficient model [14] has its own limitation, it is appropriate to verify the protection method.

To obtain accurate transient responses, a frequency dependent model for the 200km DC cables is used. The configuration of the DC cable is based on CIGRE B4-57 work [15]. The DC cable's parameters are adopted from IEC 60028, IEC 60889, and IEC 60287-1-1, which can also be found in [15].

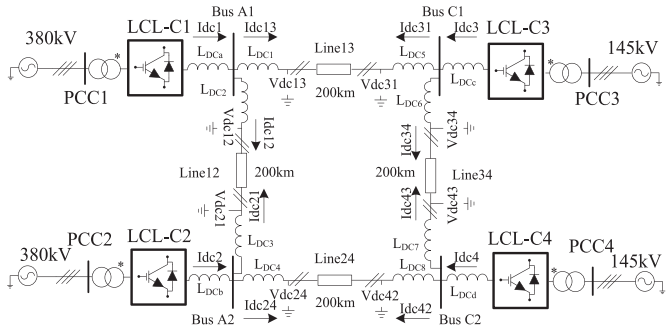

Fig. 1. A typical illustration of a terminal in an MTDC network.

TABLE I
Data of MTDC System

AC system			DC system	
Bus name	Voltage	Transformer ratio	Converter name	Control mode and setting points
PCC1	380kV	380*95%/231.58	LCL-C1	V_{dc}: V_{dc_ref}=±200kV
				Q: Q_{ref}=0 MVAR
PCC2		380*95%/231.58	LCL-C2	P/$V_{dcdroop}$: P_{ref}=-300MW, droop=0.05
				Q: Q_{ref}=0 MVAR
PCC3	145kV	145*100%/231.58	LCL-C3	P/$V_{dcdroop}$: P_{ref}=700MW, droop=0.05
				Q: Q_{ref}=0 MVAR
PCC4		145*95%/231.58	LCL-C4	P/$V_{dcdroop}$: P_{ref}=-300MW, droop=0.05
				Q: Q_{ref}=0 MVAR

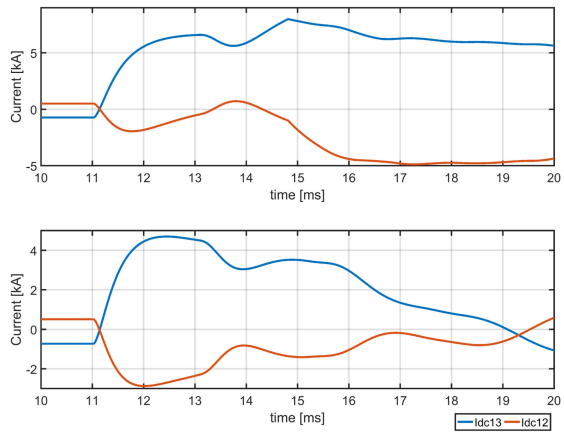

Fig. 2. Neighboring currents due to a fault on Line13. Upper plot: Pole-to-pole fault. Bottom plot: Pole-to-ground fault.

B. Currents and Voltages of Neighboring DC Lines

In Fig. 1, a current limiting inductor is installed at each terminal of the DC lines. When a fault occurs on the middle point of Line13 (which could be either a cable or an OHL), the waveforms of the neighboring currents Idc13 and Idc12 are shown in Fig. 2. It is obvious that the current measured in the faulty line would increase, whilst that measured in the healthy line would decrease. Therefore, the different current changing directions reveal an important criterion that can be used for fault detection. However, as the travelling waves can propagate toward other locations and relays, the use of current changing directions is insufficient for reliable fault detection, even when the travelling wave is attenuated by a cable or an OHL.

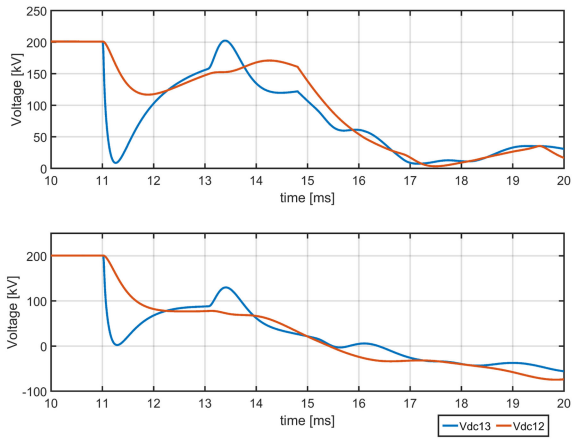

Fig. 3. Responses of voltage at the end of line to fault on Line13. Upper plot: Pole-to-pole fault. Bottom plot: Pole-to-ground fault.

Besides the current, the DC voltage can be similarly analyzed during the fault current period. In Fig. 3, the waveforms of voltages Vdc13 and Vdc12 at the ends of Line13 and Line12 are simulated and demonstrated. It can be easily proved that due to the inductive potentials of current limiters L_{DC1} and L_{DC2}, the voltage drop at the end of Line12 is delayed, and the delay time depends on the size of inductors. Therefore, the inductors at remote ends of the line can help divide the grid into different zones, as the voltages measured at the two sides of the inductor after the fault have different values. Consequently, the inductors on DC lines are also necessary for defining the protection criteria. In this study, a value of 20mH for the terminal inductor is used [16], [17]. By considering the aforementioned current characteristics, we can accurately identify a fault based on the current and voltage properties.

III. Description of the Algorithm

In Section II, the variations of the DC current and voltage after a fault occurrence are analyzed to show that a fault can be detected based on two criteria: The increase of current and the fast drop of voltage. Accordingly, a methodology for fault detection is explained, and the results of using MAD to process fault current and voltage are also shown.

A. Basic Concept of MAD and Its Performance

The median absolute deviation (MAD) method is a robust statistical method, which can locate outliers in a dataset or in a signal series [18], [19], i.e., the most abrupt value during a transient process. Assume that a signal series *W* is given containing the latest *m* samples of *X* within an observation interval:

$$W = [X(t - m \cdot \Delta t), \ldots, X(t - \Delta t)\ \ X(t)] \qquad (1)$$

where, Δt is one sampling interval. Then, the MAD of *W* is defined by (2) as the median of the absolute deviations of each dataset sample from the median of the complete *W* dataset:

$$MAD(W) = median\{|W - median(W)|\} \qquad (2)$$

Since it is unlikely that *W* has symmetrically distributed sample values (due to possible noise), it is prudent to perform MAD_{double} [20] to properly identify the high and low outliers of the dataset. The description of MAD_{double} is defined as follows:

$$MAD_{double}(W) = \begin{cases} MAD_{low} = MAD(W), W \le median(W) \\ MAD_{high} = MAD(W), W > median(W) \end{cases} \qquad (3)$$

In (3), the MAD_{low} value corresponds to the median absolute deviation from the median of all samples less than or equal to the median of the complete *W* dataset. Furthermore, MAD_{high} value corresponds to the median absolute deviation from the median of all samples greater than the median of the complete *W* dataset. Then, the MAD denominated samples of *W* can be obtained by:

$$W_{MAD} = [W - median(W)]/MAD_{double}(W) \qquad (4)$$

According to (4), it is understandable that W_{MAD} is dependent on the whole set of *W*. Therefore, after implementing a moving window function to *W*, W_{MAD} is automatically updated at each sampling interval, so only the most recent *m* samples are considered. Both the required number of samples and the sampling frequency can be defined accordingly. Furthermore, since the algorithm sorts all samples and computes the median of the dataset, the noise immunization of W_{MAD} is high.

If we inspect equations (1) to (4) of MAD, the result of W_{MAD} can increase immediately to an extremely distinguishable value [19]. The reason is that even when an outlier is recorded in the dataset, the value of (2) is still close to zero since the whole system is still in steady-state. Therefore, based on (4), W_{MAD} is theoretically infinite, which is in practice not possible due to the noise in the system; however, it still holds extremely large value. Although in [18], there is an absolute value operator in the numerator of W_{MAD}, it is removed here in (4). This allows the use of polarities (±) of MAD to identify rapidly increasing and decreasing values of the signals. Consequently, MAD becomes more effective on HVDC systems, as it detects the abrupt current change due to a DC fault.

Fig. 4 shows the results of the current signals from Fig. 2 processed by MAD. From the right axes, it can be seen that the MAD can generate distinguishably high values, which occur almost immediately after the surge arrives at 11ms. Also, the currents of neighboring healthy and faulty lines have opposite polarities of MAD. This feature serves as a fast and selective indicator to detect a DC fault: The positive output of MAD indicates the related abrupt change on the faulty line.

B. Modification of MAD

As noted in Section II, the incident surge propagates along the whole network. Hence, the fault current could be detected by MAD at other remote healthy buses. During a simulation or a practical test, there is uncertainty about the exact value of the MAD output. Consequently, it is hard to use MAD solely to establish a reliable fault detection criterion. Therefore, a second

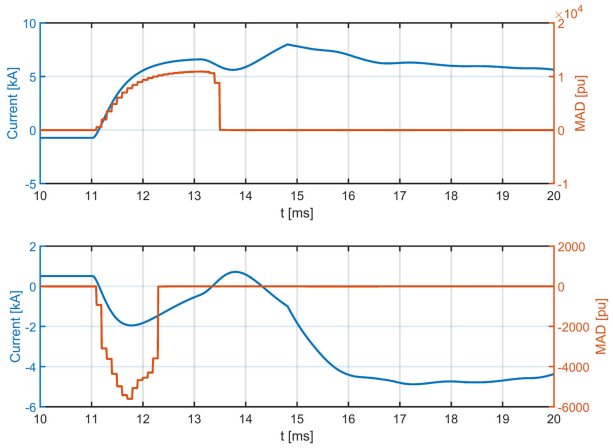

Fig. 4. Results of using MAD to process fault current. Upper plot: Idc13. Bottom plot: Idc12.

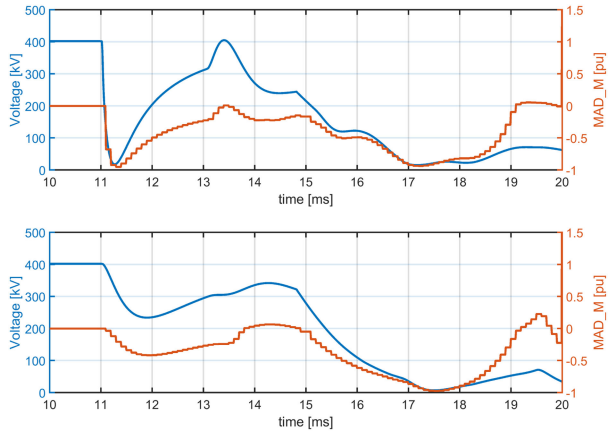

Fig. 5. Results of using MAD_M to process fault voltage. Upper plot: Vdc12. Bottom plot: Vdc13.

criterion can be added, which should be more quantifiable than MAD.

To achieve this, expression (2) is modified as:

$$MAD\_M\,(W) = median\,(W) \tag{5}$$

The other equations remain unchanged. The modified algorithm is referred as MAD_M. Like MAD, the results of using MAD_M to process voltages Vdc13 and Vdc12 from Fig. 3 are shown in Fig. 5. We can notice that the results of MAD_M for Vdc13 drops to -1 almost immediately, which is much faster than that for Vdc12. In addition, since the lowest possible value of MAD_M is -1, MAD_M is more quantifiable than MAD; thus, it would be easier when selecting thresholds for MAD_M. Consequently, the use of MAD_M to process the DC voltage is decided as another criterion.

IV. Sensitivity and Selectivity Analysis

A. Fault Detection Criteria and Thresholds

When using the MAD for protection purpose, it is necessary to consider its security and dependability within certain margins.

TABLE II
Results of Fault A for Bus A1

	Bus A1		Bus A2		Bus C1		Bus C2	
MAD	$Idc13^+$	92.61	$Idc21^+$	-4.9	$Idc31^+$	764.31	$Idc43^+$	-7.21
	$Idc13^-$	656.66	Idc21-	41.84	$Idc31^-$	5112.27	$Idc43^-$	112.43
	$Idc12^+$	113.89	$Idc24^+$	11.96	$Idc34^+$	231.14	$Idc42^+$	25.72
	Idc12-	-664.93	$Idc24^-$	-33.57	$Idc34^-$	-1052.02	$Idc42^-$	-72.88
MAD_M	$Vdc13^+$	0.0069	$Vdc21^+$	0.0062	$Vdc31^+$	0.012	$Vdc43^+$	0.0038
	$Vdc13^-$	-0.65	$Vdc21^-$	-0.029	$Vdc31^-$	-0.99	$Vdc43^-$	-0.018
	$Vdc12^+$	0.0031	$Vdc24^+$	0.003	$Vdc34^+$	0.012	$Vdc42^+$	0.0011
	$Vdc12^-$	-0.015	$Vdc24^-$	-0.0087	$Vdc34^-$	-0.055	$Vdc42^-$	-0.009

TABLE III
Results of Fault B for Bus A1

	Bus A1		Bus A2		Bus C1		Bus C2	
MAD	$Idc13^+$	34.02	$Idc21^+$	6.86	$Idc31^+$	-3640	$Idc43^+$	56.59
	$Idc13^-$		Idc21-		$Idc31^-$		$Idc43^-$	
	$Idc12^+$	-52.64	$Idc24^+$	6.06	$Idc34^+$	-1858	$Idc42^+$	-174.14
	Idc12-		$Idc24^-$		$Idc34^-$		$Idc42^-$	
MAD_M	$Vdc13^+$	-0.043	$Vdc21^+$	-0.0078	$Vdc31^+$	-0.13	$Vdc43^+$	-0.043
	$Vdc13^-$		$Vdc21^-$		$Vdc31^-$		$Vdc43^-$	
	$Vdc12^+$	-0.015	$Vdc24^+$	-0.0017	$Vdc34^+$	-0.13	$Vdc42^+$	-0.005
	$Vdc12^-$		$Vdc24^-$		$Vdc34^-$		$Vdc42^-$	

In this section, the thresholds are discussed and determined with consideration of these two factors.

The thresholds must be determined in such a way that a relay can reliably detect the faults occurring within its protection zone, and discriminating those that are out of the zone. Thus, it is necessary to analyze the sensitivity of MAD and MAD_M. In this work, they are tested for the same MTDC system shown in Fig. 1, for faults which occur at the boundary (Fault A) and outside of the protection zone (Fault B). For instance, for the relay at Bus A1, Fault A is a pole-to-ground at the end of Line 13, whilst Fault B is a pole-to-pole fault at Bus C1. The simulation results at the instant when the surge arrives are shown in Tables II and III respectively. The fault resistance in both cases is set to 0 Ω, as in the reality, the cable faults are usually bolted faults.

In Tables II and III, the '+' and '−' respectively denote the quantities measured on the positive and negative poles of the HVDC system. In addition, the currents and voltages on the faulty and healthy poles, as well as on the lines are recorded. By comparing the simulation results of the faulty poles (marked in red in Table II) with those of the healthy poles, the main criteria of the proposed protection algorithm are defined by (6) and (7):

$$MAD.I = \begin{cases} 1, W_{MAD}\,(t) \geq 400 \\ \wedge W_{MAD}\,(t) \geq 10 W_{MAD}\,(t - \Delta t) \\ 0, \text{ else} \end{cases} \tag{6}$$

$$MAD.V = \begin{cases} 1, W_{MAD\_M}\,(t) \leq -0.2 \\ \wedge W_{MAD\_M}\,(t) \leq W_{MAD\_M}\,(t - \Delta t) \\ 0, \text{ else} \end{cases} \tag{7}$$

Equations (6) and (7) correspond to the current and the voltage measured at the same end of a DC pole, respectively. A faulty pole is detected when they are both equal to 1. To activate all the required operations, thresholds of 400 and -0.2 were used. In addition, the value $W_{MAD}(t)$ for the present sampling period

should be several times higher than the value $W_{MAD}(t-\Delta t)$ for the previous sampling period. This number is a safety coefficient to identify that the $W_{MAD}(t)$ should be sufficiently large when an outlier is recorded (it cannot be infinite due to noise). Based on the data flow of W_{MAD} in simulations, the safety coefficient can be determined heuristically [21]. By contrast, because of the modification in (5), $W_{MAD\_M}(t)$ computed by (4) cannot be lower than -1, as shown in Fig. 5. Consequently, the safety coefficient is unnecessary in (7).

Due to the settings of Faults A and B when determining the thresholds, the security margin when discriminating internal and external faults is not high in Table II and Table III. Here, the thresholds are determined by making use of a cable system with parameters taken from [15]. When the protection method is implemented for an OHL system, or for a system with mixed overhead and underground cables, the thresholds would be changed by different characteristic impedances. Based on the analysis method in [22]–[24], the absolute values of the thresholds would be inversely proportional to the characteristic impedance. Also, the possible high-impedance fault in an OHL system affects the selection of thresholds.

According to the algorithm, a fault will be detected when (6) and (7) become positive at the same time. In practice, although the sampled data are discrete, the sampling of DC current and voltage can be synchronized in time. However, as a feature of EMT simulation, the branch current is always computed one time-step later than the nodal voltage, and the computation of (6) and (7) in RTDS is also time consuming. Therefore, it is unlikely that the criteria defined by (6) and (7) can be strictly fulfilled at the same instant during the simulation. Consequently, it is decided that when the criteria are satisfied, the MAD.V and MAD.I generate a square wave with one second duration and ten milliseconds duration, respectively. This guarantees that even when these two indices subsequently become 1 in a small timeframe (which can be several simulation time-steps), a trip signal will be sent to local DCCBs.

This timeframe or coordination is introduced by the RTDS limits and the consequent simulation settings, which are a tradeoff between the reliability requirement of the proposed protection method and the accuracy of the real-time simulation. Since this timeframe is unavoidable, the generation of the indices in the form of square waves is necessary to avoid protection failure. The illustration of the protection method is demonstrated in Fig. 6. As the relay unit is installed at each pole, when both units at two poles pick up, the fault is identified as a pole-to-pole fault; otherwise, it is a pole-to-ground fault. In practice, an extra starting element [7] should be considered to remove the impact of possible bad samples.

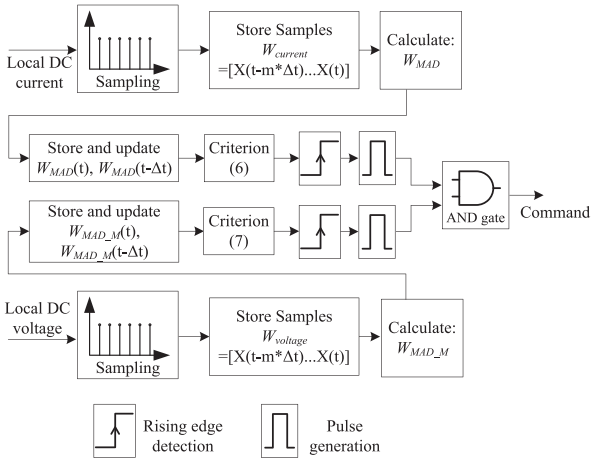

Fig. 6. A block diagram of DC fault protection.

TABLE IV
PERFORMANCE OF PROPOSED METHOD (I)

	F1				
	MAD.I		MAD.V		Command
BusA1	$Idc13^+$	1@11.1ms	$Vdc13^+$	1@11.1ms	1@11.1ms
	$Idc13^-$		$Vdc13^-$		
	$Idc12^+$	0	$Vdc12^+$	1@11.59ms	0
	$Idc12^-$		$Vdc12^-$		
BusA2	$Idc21^+$	0	$Vdc21^+$	0	0
	$Idc21^-$		$Vdc21^-$		
	$Idc24^+$	0	$Vdc24^+$	0	0
	$Idc24^-$		$Vdc24^-$		
BusC1	$Idc31^+$	1@10.1ms	$Vdc31^+$	1@10.1ms	1@10.1ms
	$Idc31^-$		$Vdc31^-$		
	$Idc34^+$	0	$Vdc34^+$	1@10.5ms	0
	$Idc34^-$		$Vdc34^-$		
BusC2	$Idc43^+$	0	$Vdc43^+$	0	0
	$Idc43^-$		$Vdc43^-$		
	$Idc42^+$	0	$Vdc42^+$	1@13ms	0
	$Idc42^-$		$Vdc42^-$		

	F2				
	MAD.I		MAD.V		Command
BusA1	$Idc13^+$	0	$Vdc13^+$	1@11.3ms	0
	$Idc13^-$	0	$Vdc13^-$	0	0
	$Idc12^+$	0	$Vdc12^+$	1@11.9ms	0
	$Idc12^-$	0	$Vdc12^-$	0	0
BusA2	$Idc21^+$	0	$Vdc21^+$	1@12.9ms	0
	$Idc21^-$	0	$Vdc21^-$	0	0
	$Idc24^+$	0	$Vdc24^+$	1@12.9ms	0
	$Idc24^-$	0	$Vdc24^-$	0	0
BusC1	$Idc31^+$	0	$Vdc31^+$	1@10.2ms	0
	$Idc31^-$	1@10.1ms	$Vdc31^-$	0	0
	$Idc34^+$	0	$Vdc34^+$	1@10.2ms	0
	$Idc34^-$	1@10.1ms	$Vdc34^-$	0	0
BusC2	$Idc43^+$	0	$Vdc43^+$	1@11.3ms	0
	$Idc43^-$	0	$Vdc43^-$	0	0
	$Idc42^+$	0	$Vdc42^+$	1@11.2ms	0
	$Idc42^-$	0	$Vdc42^-$	0	0

B. Performance of the Proposed Method

In this section, the protection method is tested by six independent fault cases:

- F1: Pole-to-pole (PtP) fault on Line13. 200 km from Bus A1.
- F2: Positive pole-to-ground (PtG) fault on Bus C1.
- F3: PtP fault on Line12. 50km from Bus A2.
- F4: PtP fault on Line24. 100 km from Bus A2.
- F5: Negative PtG fault on Line34. 60km from Bus C1,.
- F6: Negative PtG fault on Bus C1.

In all the cases, the fault was applied at 10ms and the fault resistance is 0Ω. The simulation results are listed in Tables IV and V. The signals are sampled with a frequency of 10 kHz, and

TABLE V
PERFORMANCE OF PROPOSED METHOD (II)

	RA1_13		RA1_12		RA2_12		RA2_24		RC1_13		RC1_34		RC2_34		RC2_24	
	+	-	+	-	+	-	+	-	+	-	+	-	+	-	+	-
F3	0	0	1	1	1	1	0	0	0	0	0	0	0	0	0	0
F4	0	0	0	0	0	0	1	1	0	0	0	0	0	0	1	1
F5	0	0	0	0	0	0	0	0	0	0	0	1	0	1	0	0
F6	0	0	0	0	0	0	0	0	0	0	0	0	0	0	0	0

the latest 50 samples are stored for processing. It is also assumed that at each end of a DC line, there are two relay units installed on the positive and negative poles, and all the units makes use of the protection in Fig. 6. The instants when indices MAD.I and MAD.V become 1 in F1 and F2 are listed in Table IV, whilst the commands given by the relays for test cases F3 to F6 are summarized in Table V. It should be noted that the icons in the first row of Table V correspond to the relays that are supposed to protect certain DC lines, which for instance means that RA1_13 is the relay at Bus A1 protecting Line13. As in Tables II and III, the '+' and '−' in these two tables imply positive and negative poles, respectively.

It is observable that in both Tables IV and V, only the relay units installed on the faulty line or pole will provide a command indicating a fault. However, for the healthy lines or poles, even though the fault can be detected through either the current or the voltage, there are no trip commands given. By taking the indices for BusC1 in case F2 of Table IV as an example, we can see that although the MAD.I of $Idc34^-$ becomes 1, the corresponding MAD.V of $Vdc34^-$ remains 0; hence, no command is generated for Line34's negative pole. Furthermore, all the faults on DC lines can be promptly detected in cases F3 to F5, which implies that the proposed method is highly sensitive and reliable.

V. REAL TIME DIGITAL SIMULATOR PLATFORM

To demonstrate the capabilities of the proposed algorithm, the cyber-physical simulation platform is utilized, as a co-simulation between the electric power system model and IEC 61850 based ICT infrastructure in real-time.

A. Real Time Simulation Platform

The real time cyber-physical simulation platform is illustrated in Fig. 7. The MTDC system in Fig. 1 and protection logic in Fig. 6 are firstly coded in C language as user-defined models, and then simulated in real-time using RTDS [25]. Furthermore, using the hardware (i.e., GTFPGA and GTNETx2 in Fig. 7), the sample value (SV) messaging is conducted and can be interpolated. Although these two units can support both IEC 61850-9-2LE and IEC 61869-9 standards, the proposed protection method only requires a sampling frequency of 10 kHz. Therefore, IEC 61850-9-2LE is considered, as it provides a sampling frequency of 12.8 kHz, which is sufficient for the proposed method. The SVs from the critical measuring points in the MTDC system will be sent (published) to the local Ethernet network by GTFPGA. Whilst the GTNETx2 is configured to subscribe to the SV data stream that feeds the measurements to the protection functions

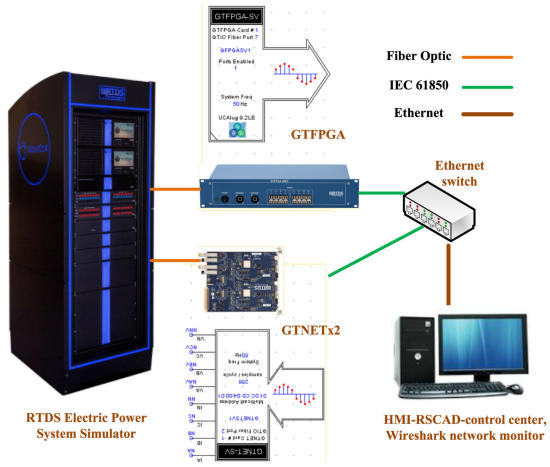

Fig. 7. Real time simulation platform based on RTDS and IEC 61850 based ICT infrastructure.

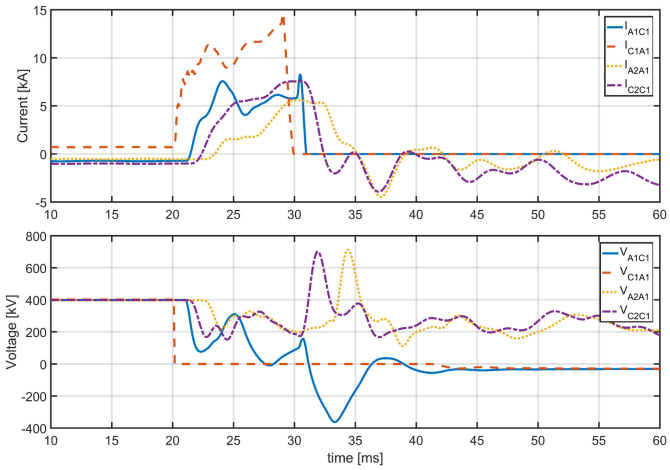

Fig. 8. Currents and voltages measured by criterial relays.

(6) and (7) established in RTDS. The corresponding data flows can be observed and analyzed by using the Wireshark network analyzer installed on the PC that is connected to the local Ethernet switch.

B. Validation of the Proposed Protective Algorithm

To validate the proposed algorithm, the fault case F1 described in Section IV.B is applied at 20ms on the platform shown in Fig. 7. The DCCB models have been implemented at each end of the DC transmission line. Four critical relays and DCCBs are selected as observed objects (RA1_13, RC1_13, RA2_12 and RC2_34), which will detect positive fault currents. When the communication delay is not considered, the simulation results with the main time-step of 75μs (VSCs and DC breakers [26] are modeled in a small time-step 3.124μs) are plotted from Fig. 8 toFig. 10. The voltage and current waveforms seen by the four critical relays and breakers are depicted in Fig. 8. In this figure, the subscripts A1C1, C1A1, A2A1, and C2C1 represent the measurement points close to buses A1, C1, A2, and C2 on related lines respectively.

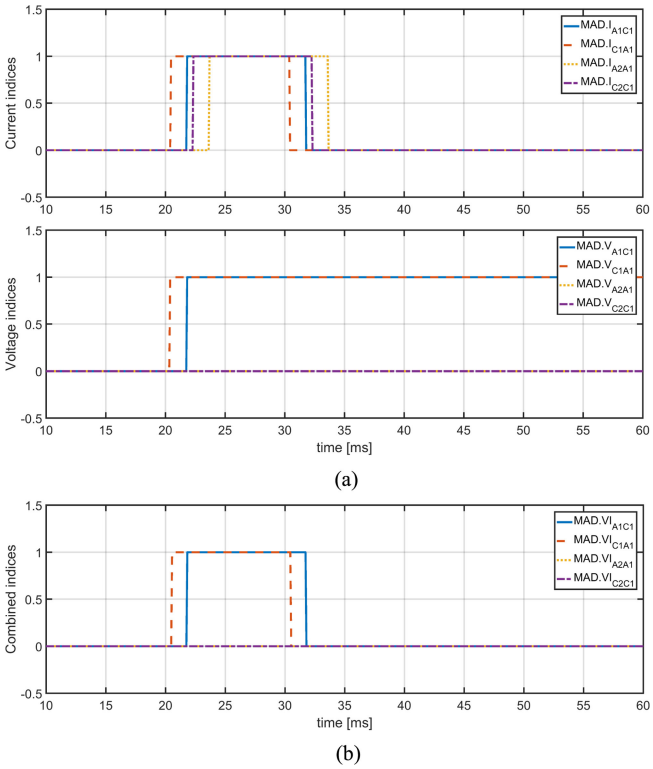

Fig. 9. Protection indices of the critical relays, (a) Current and voltage indices of critical relays, (b) Combined indices of critical relays.

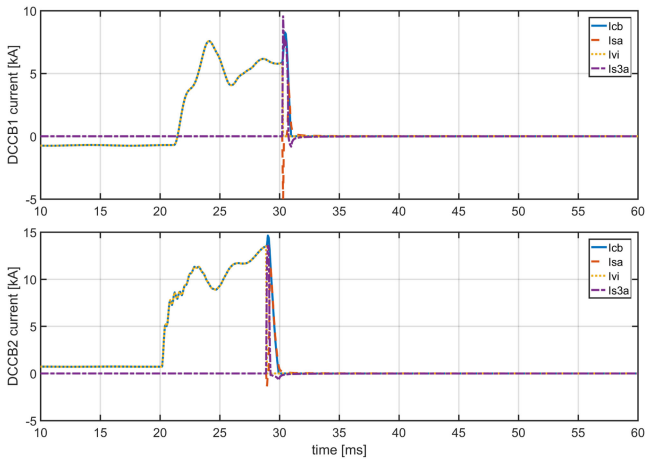

Fig. 10. Currents of DCCBs.

In the meantime, the MAD-based indices are shown in Fig. 9. It can be seen that the sensitivity of the current index (MAD.I) is higher than the voltage index (MAD.V) in Fig. 9(a), as all four relays detect the current derivations, whilst only the two relays installed on the faulty line detect the voltage derivations. The combined indices $\mathrm{MAD.VI_{A1C1}}$ and $\mathrm{MAD.VI_{C1A1}}$ generate commands to indicate the fault, which are shown in Fig. 9(b). Based on the proposed criteria and selected thresholds, the protection system in this case shows good performance in detecting and locating the fault F1 on Line13, which occurs between Bus A1 and Bus C1.

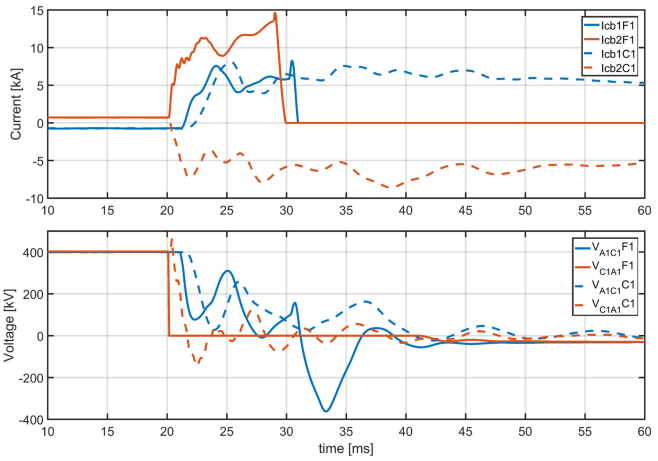

Fig. 11. Currents and voltages during the faults in C1 and C2.

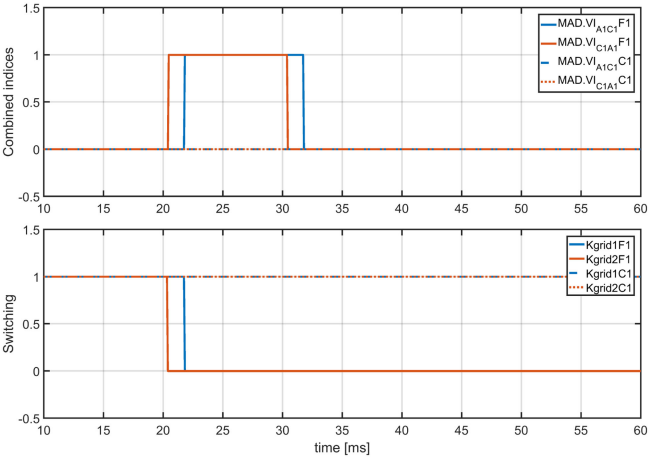

Fig. 12. Protection indices and tripping signals in C1 and C2.

When the corresponding trip signals are generated, the performance of the DCCBs can be observed from the current waveforms shown in Fig. 10. Icb, Ivi, Isa, and Is3a are the current flowing through the whole mechanical DCCB, the current of the vacuum interrupter branch, the current of surge arrestor branch, and the current of counter current injection branch, respectively [26]. Due to the different distances between the relays and the fault, the fault is detected and interrupted at different instants. Since the operation delay time of all DCCB interrupters is set to 8 ms [26], for the DCCB2, the interruption time is around 28.88ms, whilst for DCCB1 it is around 30.22 ms.

Furthermore, to give a simple observation of the sensitivity and the selectivity of the proposed protection algorithm and related criteria in RTDS, besides case F1, one more case has been simulated by the testing platform, i.e., case C1: PtP fault applied on Bus C1 at 20 ms, $\mathrm{R_F} = 0\,\Omega$. The currents and the voltages on Line13 during the faulty periods are shown in Fig. 11, and the MAD-based indices together with the associated grid tripping signal Kgrid (initiated by MAD) in both cases are shown in Fig. 12.

Fig. 12 shows that the relays with the proposed protection algorithms give good performances in the RTDS. The fault in

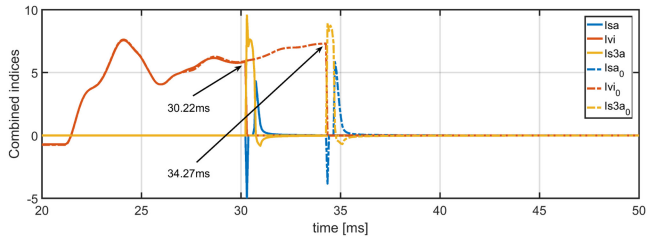

Fig. 13. Currents of DCCB1 with different delays.

TABLE VI
CRITICAL TIMINGS AND DELAYS OF DCCB1 AND PROTECTION

	Timings			Comm.
	Detection	Tripping	Interruption	Delays
Without communication	21.7ms	21.7ms	30.22ms	0ms
With communication	23.78ms	25.97ms	34.27ms	2.2ms

F1 was detected successfully, and the fault in case C1, which is located at Bus C1, was discriminated. In case C1, the current Icb1 seen by DCCB1 increases faster in the beginning, and Icb2 is negative. The voltages measured at the remote ends of Line13 drop slower in the beginning. Thus, the related indices are kept at the zero level, and the DCCBs are not tripped in case C1.

Since the communication links are based on IEC61850, its time delay affects the performance of the protection and breaker. To investigate the effects of the time delay, DCCB1 at Bus A1 is observed for fault case F1, and its performance with different communication settings is shown in Fig. 13. For easy comparison, the waveforms without subscripts indicate that the communication link is not applied. Furthermore, when the SV communication links are implemented, the related waveforms are shown with dashed lines marked by legends with subscript 0. In Fig. 13 and Table VI, it is obvious that when the communication link is applied, the fault detection takes longer time. The results shown in Fig. 13 and Table VI do not take the mechanical delay (8ms) of DCCB interruption into the final communication delays.

It should be noted that although the time delay is introduced by the communication link, the DCCBs can sustain the current during this time delay since the fault current has been limited by the LCL converter [13]. Therefore, a DCCB is not necessary to be over dimensioned as the fault current would not increase significantly during the time delay. Since the protection should normally operate within 2 ms from the fault occurrence [26], the present technology of digital information communication may not be mature enough to support all the DC protection solutions, which needs to be further upgraded. More research should be done in the near future.

VI. CONCLUSION

This paper proposes a novel protection algorithm based on the analysis of fault-caused incident surges in HVDC systems. The MAD-based method can extract the characteristics of currents and voltages at the ends of both neighboring faulty and healthy lines, immediately after the fault occurrence. Thus, with limited local samples, the proposed combined criteria can ensure the selectivity of the protection algorithm, which in this work is comprehensively demonstrated. For the proposed methodology, DC reactors are needed for DC line fault detection and for designing zonal protection scheme, even though DC reactors on the DC line is mainly used for limiting the rate of rise of the DC fault current.

The proposed algorithm is successfully coded using Fortran and C. Therefore, it can be flexibly installed on a hardware platform by sampling the required current and voltage as input parameters. By defining a window with a length of N samples per signal, for each time-step, MAD.V and MAD.I are computed according to (6) and (7). At the same time, the window is updated by a new sample whilst the oldest sample is omitted from the window. This allows fast computation and low memory burden. This is however, beyond the scope of this work and will be a challenge for future research work.

The proposed protection method was validated using a cyber-physical simulation platform developed on the RTDS platform. At the same time, an SV-based protocol was adopted to provide the required sampling frequency and communication interfaces. The real-time simulation cases demonstrate that the proposed method is highly robust and considers the latency introduced by hardware interfacing, data communication and processing when implementing SV protocols. Even though the implemented SV messaging link may not be suitable for DC protection applications, the proposed method can be realized effectively with future technologies, due to its relaxed requirements. Since the protection method needs local signal processing at a DC bus station, more improvements and implementation of information communication technologies are necessary. Then, the proposed protection method will be a valuable addition to the concept of the digital substation.

REFERENCES

[1] M. van der Meijden, "Future North Sea infrastructure based on Dogger Bank Modular Island," presented at 15th Wind Integration Workshop, pp. 1–3, Nov. 2016.
[2] Y. Pipelzadeh *et al.*, "Modelling and dynamic operation of the Zhoushan DC grid: World's first five-terminal VSC-HVDC project," in *Proc. Int. High Voltage Direct Current Conf.*, 2015, pp. 87–95.
[3] R. Li *et al.*, "A hybrid modular multilevel converter with novel three-level cells for DC fault blocking capability," *IEEE Trans. Power Del.*, vol. 30, no. 4, pp. 2017–2026, Aug. 2017.
[4] M. Hajian, L. Zhang, and D. Jovcic, "DC transmission grid with low-speed protection using mechanical DC circuit breakers," *IEEE Trans. Power Del.*, vol. 30, no. 3, pp. 1381–1391, Jun. 2015.
[5] G. Zou *et al.*, "A fast protection scheme for VSC based multi-terminal DC grid," *Int. J. Elect. Power Energy Syst.*, vol. 98, pp. 307–314, Jun. 2018.
[6] K. De Kerf *et al.*, "Wavelet-based protection strategy for DC faults in multi-terminal VSC HVDC systems," *IET Gener., Transmiss. Distrib.*, vol. 5, no. 4, pp. 496–503, Jan. 2011.
[7] F. Kong, Z. Hao, S. Zhang, and B. Zhang, "Development of a novel protection device for bipolar HVDC transmission lines," *IEEE Trans. Power Del.*, vol. 29, no. 5, pp. 2270–2278, Oct. 2014.
[8] W. Leterme, J. Beerten, and D. V. Hertem, "Non-unit protection of HVDC grids with inductive DC cable termination," *IEEE Trans. Power Del.*, vol. 31, no. 2, Apr. 2016.
[9] J. Suonan, J. Zhang, Z. Jiao, L. Yang, and G. Song, "Distance protection for HVDC transmission lines considering frequency-dependent parameters," *IEEE Trans. Power Del.*, vol. 28, no. 2, pp. 723–732, Apr. 2013.
[10] G. Song, X. Chu, S. Gao, X. Kang, and Z. Jiao, "A new whole-line quick-action protection principle for HVDC transmission lines using one-end current," *IEEE Trans. Power Del.*, vol. 20, no. 2, pp. 599–607, Apr. 2015.

[11] J. Sneath and A. Rajapakse, "Fault detection and interruption in an earched HVDC grid using ROCOV and hybrid DC breakers," *IEEE Trans. Power Del.*, vol. 31, no. 3, pp. 971–981, Jun. 2016.
[12] Technical Brochure 739, Protection and local control of DC grids, WG B4/B5.59, www.e-cigre.org, 2018.
[13] L. Liu, M. Popov, M. van der Meijden, and V. Terzija, "Optimized control of LCL-VSC converter with refined s-parameter," *IEEE Trans. Power Del.*, vol. 32, no. 4, pp. 2101–2110, Aug. 2017.
[14] U. N. Gnanarathna, A. M. Gole, and R. P. Jayasinghe, "Efficient modeling of modular multilevel HVDC converters (MMC) on electromagnetic transient simulation programs," *IEEE Trans. Power Del.*, vol. 26, no. 1, pp. 316–324, Jan. 2011.
[15] Technical Brochure 604, Guide for the development of models for HVDC converters in a HVDC grid, WG B4.57, www.e-cigre.org, 2014.
[16] R. Li, L. Xu, and L. Yao, "DC fault detection and location in meshed multiterminal HVDC systems based on DC reactor voltage change rate," *IEEE Trans. Power Del*, vol. 32, no. 3, pp. 1516–1526, Jun. 2017.
[17] W. Leterme, N. Ahmed, L. Ängquist, J. Beerten, D. Van Hertem, and S. Norrga, "A new HVDC grid test system for HVDC grid dynamics and protection studies in EMTP," in *11th IET Int. Conf. AC DC Power Transmiss.*, 2015, pp. 1–7.
[18] C. Leys *et al.*, "Detecting outliers: Do not use standard deviation around the mean, use absolute deviation around the median," *J. Exp. Social Psychol.*, vol. 49, no. 4, pp. 764–766, Jul. 2013.
[19] M. Naglic *et al.*, "Synchronized measurement technology supported AC and HVDC online disturbance detection," *Electric Power Syst. Res.*, vol. 160, pp. 308–317, Jul. 2018.
[20] P. Rosenmai, "Using the median absolute deviation to find outliers," Nov. 2013. [Online], Available: http://http://eurekastatistics.com/using-the-median-absolute-deviation-to-find-outliers/
[21] M. Naglic *et al.*, "Synchronized measurement technology supported AC and HVDC online disturbance detection," in *Proc. Int. Conf. Power Syst. Transients*, 2017, pp. 1–6.
[22] L. van der Sluis, *Transients in Power Systems*. Hoboken, NJ, USA: Wiley, 2001.
[23] E. W. Kimbark, "Transient overvoltages caused by monopolar ground fault on bipolar DC line: Theory and simulation," *IEEE Trans. Power App. Syst.*, vol. PAS-89, no. 4, pp. 584–592, Apr. 1970.
[24] N. A. Belda, C. Plet, and R. P. P. Smeets, "Analysis of faults in multi terminal HVDC grid for definition of test requirements of HVDC circuit breakers," *IEEE Trans. Power Del.*, vol. 33, no. 1, pp. 403–411, Feb. 2018.
[25] RTDS Technologies Inc., 2019. [Online]. Available: http://www.rtds.com
[26] S. Liu and M. Popov, "Development of HVDC system-level mechanical circuit breaker model," *Int. J. Elect. Power Energy Syst.*, vol. 103, pp. 159–167, Dec. 2018.

Lian Liu received the bachelor's and master's degrees in electrical engineering from Wuhan University, Wuhan, China, in 2010 and 2013, respectively, and the Ph.D. degree from the Department of Electrical Sustainable Energy, Delft University of Technology, Delft, The Netherlands, in 2019. His Ph.D. project was financed by China Scholarship Council. From 2017 to 2018, he was a Research Associate with the Department of Electrical Sustainable Energy, Delft University of Technology. His research interests include the modeling large scale of HVdc system, HVdc system transients, and power system protection.

Zhou Liu (Senior Member, IEEE) received the Ph.D. degree in energy technology from Aalborg University, Aalborg, Denmark, in 2013. Since December 2014, he has been a Postdoc Researcher with the Department of Electrical Power Engineer, Norwegian University of Science and Technology, Trondheim, Norway. From 2017 to 2018, he was a Postdoc Fellow with the Department of Electrical Sustainable Energy, TU Delft, Delft, The Netherlands. He is currently an Assistant Professor with the Department of Energy Technology, Aalborg University. His main research interests include power system protection, power system stability and control, energy system integration, digital substation, and smart grid technology.

Marjan Popov (Senior Member, IEEE) received the Dipl.Ing. degree in electrical power engineering from the University of Saints Cyril and Methodius, Skopje, Republic of Macedonia, in 1993, and the Ph.D. degree in electrical power engineering from the Delft University of Technology, Delft, The Netherlands, in 2002. He is a Chevening alumnus and in 1997, he was an Academic Visitor with the University of Liverpool, Liverpool, U.K., working with the Arc Research Group on modeling SF6 circuit breakers. His major fields of interest include future power systems, large-scale power system transients, intelligent protection for future power systems, and wide-area monitoring and protection. He is a member of CIGRE and actively participated in WG C4.502 and WG A2/C4.39. He was the recipient of the prestigious Dutch Hidde Nijland Prize for extraordinary research achievements in 2010. He was also the recipient of IEEE PES Prize Paper Award and IEEE Switchgear Committee Award in 2011. He is an Associate Editor for the Elsevier's *International Journal of Electric Power and Energy Systems*.

Peter Palensky (Senior Member, IEEE) was born in Austria in 1972. He received the M.Sc. degree in electrical engineering and the Ph.D. degree from the Vienna University of Technology, Vienna, Austria, in 1997 and 2001, respectively. He cofounded Envidatec, a German startup on energy management and analytics, and joined the Lawrence Berkeley National Laboratory, Berkeley, CA, USA, as a Researcher, and the University of Pretoria, Pretoria, South Africa, in 2008. In 2009, he became the Appointed Head of business unit on sustainable building technologies with the Austrian Institute of Technology (AIT), and later the first Principle Scientist for complex energy systems with the AIT. In 2014, he was appointed as a Full Professor for intelligent electric power grids with TU Delft. His main research fields include energy automation networks, smart grids, and modeling intelligent energy systems. He is active in international committees, such as ISO or CEN and serves an IEEE IES AdCom member-at-large in various functions for the IEEE. He is an Editor-in-Chief for the *IEEE Industrial Electronics Magazine*, an Associate Editor for several other IEEE publications, and regularly organizes IEEE conferences.

Mart A. M. M. van der Meijden (Member, IEEE) received the M.Sc. degree (*cum laude*) in electrical engineering from the Eindhoven University of Technology, Eindhoven, The Netherlands, in 1981. He has been a Full Professor (part-time) with the Department of Electrical Sustainable Energy, Faculty of Electrical Engineering, Mathematics and Computers Science, Delft University of Technology, Delft, The Netherlands, since June 2011. Since 2003, he has been with TenneT TSO, Arnhem, The Netherlands, Europe's first cross-border grid operator for electricity. He is currently a Manager R&D/Innovation and was responsible for the development of the TenneT long-term vision on the electrical transmission system. His chair and research focus is on large-scale sustainable power systems. He has more than 30 years of working experience in the field of process automation and the transmission and the distribution of gas, district heating, and electricity. He is leading research programs on intelligent electrical power grids, reliable and large-scale integration of renewable (wind and solar) energy sources in the European electrical power systems and advanced grid concepts. He is a member of ENTSO-E/RDIC and CIGRE and he has joined and chaired different national and international expert groups.